CHINESE OPTICS LETTERS

Vol. 23, No. 5 | May 2025

Optical isolator in a ferromagnetic microsphere coupled integrated Si_3N_4 waveguide

Hongyi Qiao (乔弘毅)[1,3], Shuai Wan (万 帅)[1,3], Guanting Xu (徐冠庭)[1,3], Zhen Shen (沈 镇)[1,3], Guangcan Guo (郭光灿)[1,3], Shuiming Hu (胡水明)[2,3*], and Chunhua Dong (董春华)[1,3**]

[1] CAS Key Laboratory of Quantum Information, University of Science and Technology of China, Hefei 230026, China

[2] Department of Chemical Physics, University of Science and Technology of China, Hefei 230026, China

[3] CAS Center for Excellence in Quantum Information and Quantum Physics, University of Science and Technology of China, Hefei 230026, China

*Corresponding author: smhu@ustc.edu.cn

**Corresponding author: chunhua@ustc.edu.cn

Received September 23, 2024 | Accepted November 12, 2024 | Posted Online April 30, 2025

We experimentally demonstrate an optical isolator utilizing high-quality-factor whispering gallery modes in a yttrium iron garnet (YIG) microsphere, coupled with an integrated Si_3N_4 waveguide. By applying a magnetic field in the vertical direction of the resonator equator, we achieve the breaking of degeneracy between the clockwise (CW) and counterclockwise (CCW) modes, driven by photonic spin–orbit coupling (SOC) and the Faraday effect. The maximum wavelength separation observed is about 7.9 pm, comparable with the linewidth of the mode. The better effect of the refractive index matching between the YIG microsphere and the Si_3N_4 waveguide enables an isolation ratio of 16.9 dB under the critical coupling condition. This work presents a novel integrated approach for realizing non-reciprocity in photonic circuits, advancing the development of compact high-performance photonic devices.

Keywords: yttrium iron garnet microsphere; optical isolator; Si_3N_4 waveguide.
DOI: 10.3788/COL202523.052601

1. Introduction

Non-reciprocal devices, such as isolators and circulators, are widely used due to their unidirectional transmission properties, which are particularly effective for blocking undesired eflections and guiding light along designated pathways[1–6]. Conventionally, non-reciprocity is achieved through the Faraday effect in magneto-optical (MO) materials[7]. However, this approach is constrained by the finite strength of the magnetic field and the Verdet constant, and it typically necessitates a long optical path, which complicates integration[7,8]. To solve this challenge, MO material-based cavities[2,9–14] have been explored to enhance light–matter interaction within high-Q resonators[15,16]. However, the obstacle to this method is that the Faraday effect from all directions will be canceled out in a uniform MO resonator for standing waves or closed-loop traveling waves and thus non-reciprocity will not be exhibited. Several strategies have been proposed to circumvent this limitation, including hybrid structures[2,17–19] or non-uniform magnetic fields[14,20,21], though these approaches often increase system complexity.

Recent studies of whispering gallery modes (WGM) in microstructures have revealed another possibility for breaking the symmetry of closed optical paths through photonic spin–orbit coupling (SOC)[22–27]. When light propagates in the microcavity, SOC emerges from the strong lateral confinement of the microcavity, generating new electric field components that alter the polarization state. For clockwise (CW) and counterclockwise (CCW) WGMs, these polarization differences lead to variations in their MO effects, resulting in a resonant frequency shift when an external magnetic field is applied perpendicular to the propagation direction. Although SOC-induced non-reciprocity has been theoretically proposed and experimentally demonstrated[26–29], related applications, such as high-performance isolators, have yet to be fully realized, particularly in systems utilizing high-refractive-index waveguides, where achieving critical coupling for optical WGMs is relatively straightforward[30]. The essential attainment of coupling plays a crucial role in enhancing the isolation performance of cavity-type isolators.

In this study, we have demonstrated the non-reciprocal phenomena in a uniform YIG microsphere coupled with an integrated silicon nitride (Si_3N_4) waveguide, subjected to a bias magnetic field with the perpendicular direction of the light path. The wavelength shift between CW and CCW modes is significant and can be finely controlled via the magnetic field. Importantly, this wavelength separation increases with the size

of the microspheres, reaching a maximum measured value of approximately 7.9 pm under optimal conditions, indicating strong potential for broadband non-reciprocal photonic devices. Benefiting from the effect of the refractive index matching between the YIG microsphere and the Si_3N_4 waveguide, we have achieved an optical isolator operating at telecom wavelengths with a maximum isolation ratio of 16.9 dB in the critical coupling regime. Such isolators exhibit outstanding performance and hold significant promise for the development of integrated non-reciprocal photonic devices.

2. Experimental Result

Figure 1 illustrates the schematic of our experimental setup for measuring the non-reciprocal behavior in the YIG microsphere, which is glued to an optical fiber tip[28,31,32]. The Si_3N_4 device is fabricated from the high-quality Si_3N_4 film consisting of a 720 nm layer, a 4 μm wet oxidation silicon dioxide (SiO_2) layer, and a 500 μm silicon substrate[33]. The waveguide features a cross section with a depth of 720 nm and a width of 2200 nm. Additionally, a ring cavity with a radius of 112 μm is fabricated on the chip, corresponding to a free spectral range (FSR) of approximately 200 GHz. The resonant modes of this ring cavity can serve as the reference modes, which are not affected by the bias magnetic field. To increase the coupling efficiency between the waveguide and the lensed fiber, a layer of SiO_2 is deposited on the edges of the chip using the plasma enhanced chemical vapor deposition (PECVD), as shown in the Fig. 1. Then, the coupling efficiency can be obtained as approximately 3 dB per facet. The coupling gap between the YIG microsphere and the waveguide can be precisely adjusted using a nano-positioning stage. The magnetic field is aligned with the stem of the microsphere, which has an angle of θ: 40°–45° to the plane of the waveguide chip to obtain the best experimental phenomena[27]. As for the light path, a tunable laser is launched into a 2×2 optical switch, which has two statuses, and controls the direction of the light passing through the waveguide and thus also determines whether the CW or CCW modes of the YIG microsphere are excited. In either case, the transmission signal will come back to the switch and be measured by a photodetector, with results displayed on the oscilloscope. A signal generator provides a sawtooth wave for the laser to finely scan the wavelength, and two fiber polarization controllers help us obtain the same polarization for these two opposite propagation directions.

Figure 2 shows the typical spectra for the TE and TM modes, with the same frequency of the CW and CCW modes. The black and orange lines are the CW and CCW modes of the Si_3N_4 microring resonator without the YIG microsphere. They are overlapped, indicating negligible influence from the magnetic field. The loaded Q factor of the Si_3N_4 microring is about 2.9×10^5. When the YIG microsphere is brought into contact with the waveguide, numerous optical modes emerge. The CW and CCW transmission spectra exhibit a distinct wavelength separation, indicating non-reciprocal transmission. Meanwhile, the CW and CCW optical modes of the Si_3N_4 resonator remain degenerate. The loaded Q factor for the TM optical mode in the YIG microsphere is 3.1×10^5, which is similar to previous works[28,31,32]. For certain optical modes, critical coupling is observed. Notably, for the TE modes, the wavelength shift occurs in the opposite direction compared to the TM modes, which can be attributed to the opposite chirality of the differently polarized modes[27].

Furthermore, the relationship between the transmission and magnetic field intensity is investigated, as indicated in Fig. 3. The intensity of the magnetic field is varied by adjusting the distance between the magnets and the YIG microsphere, with calibration performed using a magnetometer. Figure 3(a) shows the transmission evolution of a 1000-μm-diameter microsphere as the magnetic field intensity increases, providing more detailed insights. Due to the Voigt effect, the whole transmissions shift

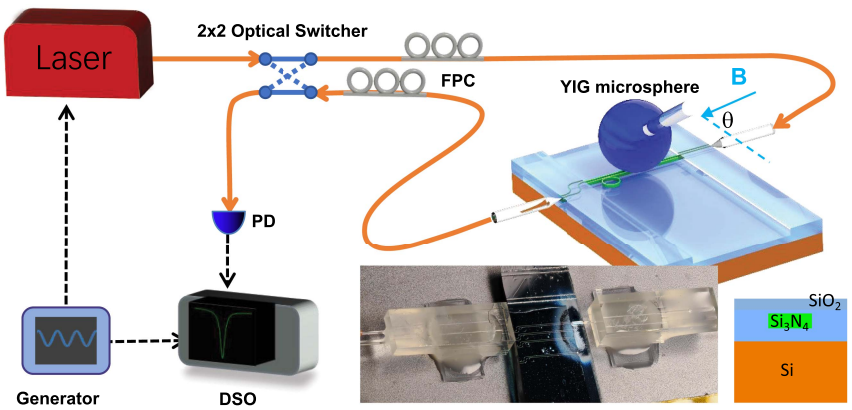

Fig. 1. Schematic of the experimental setup. The CW or CCW modes of the microsphere are probed by switching the opposite propagating lights through a 2×2 optical switcher. The bias magnetic field is perpendicular to the equator of the YIG microsphere. FPC, fiber polarization controller; DSO, digital oscilloscope; PD, photodetector. B stands for the magnetic field. Insets: the packaged Si_3N_4 waveguide and microring with the fiber lenses and the schematic cross-section view of the bus waveguide after depositing the SiO_2 for protection.

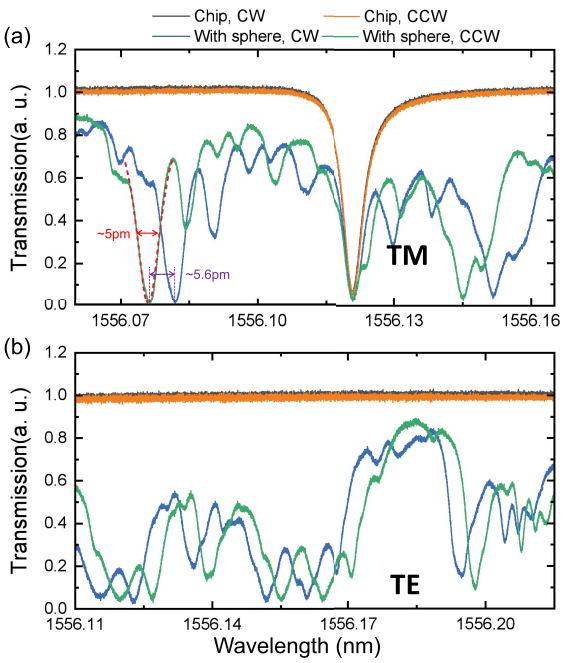

Fig. 2. Typical transmission spectra of the (a) TM- and (b) TE-polarized lights before or after the YIG microsphere touches the Si_3N_4 waveguide. The YIG microsphere has a diameter of 1000 μm with a bias magnetic field of about 50 mT.

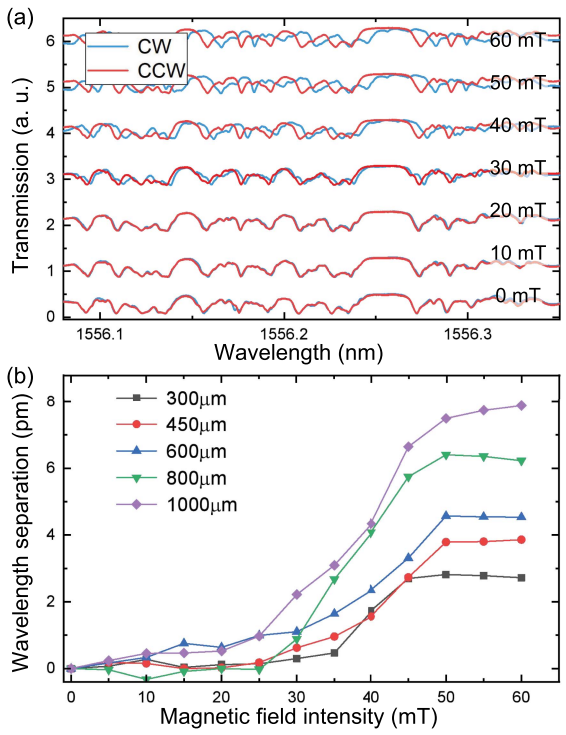

Fig. 3. (a) Transmission evolution of the 1000-μm-diameter microsphere as the magnetic field intensity increases. (b) The variation of the wavelength separation with the increase of the magnetic field intensity for microspheres with different diameters.

to the longer wavelength, which is related to the polarization[34]. For statistical analysis, these wavelength separations are calculated using the least squares method and represented by the purple line in Fig. 3(b). It is clear that with increasing magnetic field intensity, the wavelength separation between the CW and CCW modes initially appears gradually and then increases rapidly, reaching saturation at approximately 50 mT. In addition, the size of the microsphere plays a crucial role. In Fig. 3(b), various lines represent YIG microspheres with diameters ranging from 300 to 1000 μm, including the previously mentioned purple line. These results exhibit similar growth trends with all microspheres reaching saturation at nearly the same magnetic field intensity. Notably, larger microspheres have a higher upper limit of frequency shift.

When the wavelength separation between the CW and CCW modes is sufficiently large, the directional dependence of transmittance becomes more pronounced. This wavelength separation enables the realization of high-performance isolators. By matching the optical mode linewidth to the mode separation at a specific wavelength, both the isolation and the bandwidth can be optimized. To improve the isolation performance, critical coupling is another decisive factor, which is considered in our material selection. The similar refractive index of the YIG ($n = 2.19$) and Si_3N_4 ($n = 2.0$) facilitates achieving critical coupling while maintaining low loss. Additionally, expanding mode separation further increases the bandwidth limit of the isolator. To maximize the mode separation, the magnetic field is applied with an intensity above the saturation, and the largest 1000-μm-diameter microsphere is used. Under these optimal conditions, an appropriate mode is identified to demonstrate the optical isolation capabilities of the system, as shown in Fig. 4. The CW and CCW modes, represented by the blue and green lines, are almost completely separated, with the mode's linewidth closely matching the frequency separation. At the locations indicated in the figure, critical coupling is achieved for the CCW mode, while the CW mode maintains a low loss. The isolation ratio here is calculated as 16.9 dB with an insertion loss of approximately 1.40 dB.

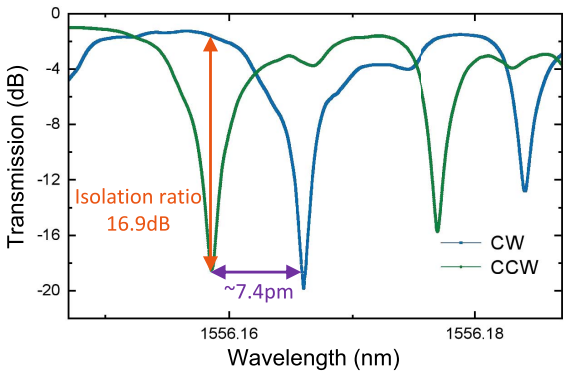

Fig. 4. Realization of isolation in the 1000-μm-diameter YIG microsphere with a bias magnetic field of about 70 mT.

3. Conclusion

In summary, we have demonstrated a non-reciprocal phenomenon within the YIG microsphere, manifested as a wavelength separation between the CW and CCW modes, which forms the basis for realizing an efficient optical isolator. By selecting Si_3N_4, the material with a closely matched refractive index of the YIG, we enhanced coupling efficiency and systematically explored the relationships among the wavelength separation, the intensity of the applied magnetic field, and the size of the microsphere. Our study shows that the isolator can achieve an isolation ratio of up to 16.9 dB with an insertion loss of approximately 1.40 dB, making it highly suitable for integration into advanced photonic circuits. Future research will focus on enhancing the capabilities of the isolator by refining fabrication techniques and investigating alternative material systems that could offer superior isolation properties or reduced insertion losses.

Disclosures

The authors declare no conflicts of interest.

Acknowledgements

This work was supported by the National Natural Science Foundation of China (Nos. 92250302, 11934012, 12104442, and 12474394), the Natural Science Foundation of Anhui Province (No. 2308085J12), and the Fundamental Research Funds for the Central Universities. This work was partially carried out at the USTC Center for Micro and Nanoscale Research and Fabrication.

References

1. Z. Yu and S. Fan, "Complete optical isolation created by indirect interband photonic transitions," Nat. Photonics **3**, 91 (2009).
2. L. Bi, J. Hu, P. Jiang, *et al.*, "On-chip optical isolation in monolithically integrated non-reciprocal optical resonators," Nat. Photonics **5**, 758 (2011).
3. Y. Shoji and T. Mizumoto, "Magneto-optical non-reciprocal devices in silicon photonics," Sci. Technol. Adv. Mater. **15**, 014602 (2014).
4. D. L. Sounas and A. Alù, "Non-reciprocal photonics based on time modulation," Nat. Photonics **11**, 774 (2017).
5. S. Maayani, R. Dahan, Y. Kligerman, *et al.*, "Flying couplers above spinning resonators generate irreversible refraction," Nature **558**, 569 (2018).
6. Y. Chen, Y.-L. Zhang, Z. Shen, *et al.*, "Synthetic gauge field in a single optomechanical resonator," Phys. Rev. Lett. **126**, 123603 (2021).
7. K. Tanaka, K. Fujita, N. Matsuoka, *et al.*, "Large Faraday effect and local structure of alkali silicate glasses containing divalent europium ions," J. Mater. Res. **13**, 1989 (1998).
8. K. J. Carothers, R. A. Norwood, and J. Pyun, "High Verdet constant materials for magneto-optical faraday rotation: A review," Chem. Mater. **34**, 2531 (2022).
9. J. Stone, R. Jopson, L. Stulz, *et al.*, "Enhancement of faraday rotation in a fibre Fabry-Perot cavity," Electron. Lett. **26**, 849 (1990).
10. H. Ling, "Theoretical investigation of transmission through a faraday-active Fabry–Perot étalon," JOSA A **11**, 754 (1994).
11. R. Rosenberg, C. Rubinstein, and D. Herriott, "Resonant optical Faraday rotator," Appl. Opt. **3**, 1079 (1964).
12. L. Dong, H. Jiang, H. Chen, *et al.*, "Enhancement of Faraday rotation effect in heterostructures with magneto-optical metals," J. Appl. Phys. **107**, 093101 (2010).
13. Y. Li, D. Steuerman, J. Berezovsky, *et al.*, "Cavity enhanced Faraday rotation of semiconductor quantum dots," Appl. Phys. Lett. **88**, 193126 (2006).
14. T. Zhang, W. Zhou, Z. Li, *et al.*, "Reversible optical isolators and quasi-circulators using a magneto-optical Fabry–Pérot cavity," Chin. Phys. Lett. **41**, 044205 (2024).
15. K. J. Vahala, "Optical microcavities," Nature **424**, 839 (2003).
16. J. Liu, F. Bo, L. Chang, *et al.*, "Emerging material platforms for integrated microcavity photonics," Sci. China Phys. Mech., and Astron. **65**, 104201 (2022).
17. W. Yan, Y. Yang, S. Liu, *et al.*, "Waveguide-integrated high-performance magneto-optical isolators and circulators on silicon nitride platforms," Optica **7**, 1555 (2020).
18. P. Pintus, D. Huang, P. A. Morton, *et al.*, "Broadband TE optical isolators and circulators in silicon photonics through Ce: YIG bonding," J. Lightwave Technol. **37**, 1463 (2019).
19. W. Šmigaj, J. Romero-Vivas, B. Gralak, *et al.*, "Magneto-optical circulator designed for operation in a uniform external magnetic field," Opt. Lett. **35**, 568 (2010).
20. M.-C. Tien, T. Mizumoto, P. Pintus, *et al.*, "Silicon ring isolators with bonded nonreciprocal magneto-optic garnets," Opt. Express **19**, 11740 (2011).
21. Z. Wang and S. Fan, "Optical circulators in two-dimensional magneto-optical photonic crystals," Opt. Lett. **30**, 1989 (2005).
22. C. Sayrin, C. Junge, R. Mitsch, *et al.*, "Nanophotonic optical isolator controlled by the internal state of cold atoms," Phys. Rev. X **5**, 041036 (2015).
23. R. Mitsch, C. Sayrin, B. Albrecht, *et al.*, "Quantum state-controlled directional spontaneous emission of photons into a nanophotonic waveguide," Nat. Commun. **5**, 5713 (2014).
24. K. Y. Bliokh, D. Smirnova, and F. Nori, "Quantum spin hall effect of light," Science **348**, 1448 (2015).
25. H. Shi, Y. Cheng, Z. Yang, *et al.*, "Optical isolation induced by subwavelength spinning particle via spin-orbit interaction," Phys. Rev. B **103**, 094105 (2021).
26. J. Ma, X. Xi, Z. Yu, *et al.*, "Hybrid graphene/silicon integrated optical isolators with photonic spin–orbit interaction," Appl. Phys. Lett. **108**, 151103 (2016).
27. C.-Z. Chai, H.-Q. Zhao, H. X. Tang, *et al.*, "Non-reciprocity in high-q ferromagnetic microspheres via photonic spin–orbit coupling," Laser Photonics Rev. **14**, 1900252 (2020).
28. X. Zhang, N. Zhu, C.-L. Zou, *et al.*, "Optomagnonic whispering gallery microresonators," Phys. Rev. Lett. **117**, 123605 (2016).
29. A. Osada, R. Hisatomi, A. Noguchi, *et al.*, "Cavity optomagnonics with spin-orbit coupled photons," Phys. Rev. Lett. **116**, 223601 (2016).
30. Z. Shen, Y.-L. Zhang, Y. Chen, *et al.*, "Reconfigurable optomechanical circulator and directional amplifier," Nat. Commun. **9**, 1797 (2018).
31. C.-Z. Chai, Z. Shen, Y.-L. Zhang, *et al.*, "Single-sideband microwave-to-optical conversion in high-q ferrimagnetic microspheres," Photonics Res. **10**, 820 (2022).
32. Z. Shen, G.-T. Xu, M. Zhang, *et al.*, "Coherent coupling between phonons, magnons, and photons," Phys. Rev. Lett. **129**, 243601 (2022).
33. S. Wan, R. Niu, J.-L. Peng, *et al.*, "Fabrication of the high-q si3n4 microresonators for soliton microcombs," Chin. Opt. Lett. **20**, 032201 (2022).
34. J. Haigh, S. Langenfeld, N. Lambert, *et al.*, "Magneto-optical coupling in whispering-gallery-mode resonators," Phys. Rev. A **92**, 063845 (2015).